IMAGING METHODOLOGY – Communication

Magnetic Resonance in Medicine 65:51–59 (2011)

Imaging Left Ventricular Tissue Mechanics and Hemodynamics During Supine Bicycle Exercise Using a Combined Tagging and Phase-Contrast MRI Pulse Sequence

Smita Sampath,[1]* John Andrew Derbyshire,[1] Maria J. Ledesma-Carbayo,[2,3] and Elliot R. McVeigh[1]

Imaging the left ventricular mechanical and hemodynamic response to the stress of exercise may offer early prognosis in select patients with cardiac disease. Here, we demonstrate the feasibility of obtaining simultaneous measurements of longitudinal strain and transvalvular blood velocity during supine bicycle exercise stress in a wide bore magnetic resonance scanner. Combining information from the two datasets, we observe that although the time to peak strain (33.28 ± 1.86 versus 25.7 ± 2.12 as % of R–R interval) and time to peak mitral inflow velocity (44.37 ± 5.21 versus 35.5 ± 4.19 as % of R–R interval) from R-wave of the QRS complex occurred earlier during stress, the time from peak strain to peak mitral inflow velocity was not statistically different (16.5 ± 3.23 versus 13.4 ± 3.06). Further, the percentage of longitudinal relaxation at peak mitral inflow velocity was higher during stress (63.5 ± 7.72 versus 84.32 ± 6.24). These results suggest that although diastole is shortened, early diastolic filling efficiency is augmented during exercise stress in normal volunteers in an effort to maintain stroke volume. Magn Reson Med 65:51–59, 2011. © 2010 Wiley-Liss, Inc.

Key words: bicycle exercise; stress; tagging; phase-contrast; SPAMM

Detecting abnormalities in left ventricular (LV) mechanical and hemodynamic response to the stress of exercise may provide early diagnostic indicators in patients suffering from valvular disease, such as ischemic mitral regurgitation, or in patients presenting with diastolic dysfunction (1,2). In some cases, pharmacological stress tests are not ideal because of reduced loading conditions, making exercise stress testing the preferred stress mechanism (3,4). Nuclear single photon emission computed tomography (SPECT) myocardial perfusion imaging is the most commonly used stress test in the clinic today, but these tests rely on estimating perfusion defects in the muscle and do not provide information on subsequent impairment in myocardial or hemodynamic function. Ultrasound-based imaging methods have been gaining importance in providing such an evaluation in patients with valvular disease. However, decreased signal to noise ratio in the images (5) and increased motion-related artifacts (6) during exercise stress echocardiography have been reported. Although it is unlikely that magnetic resonance (MR) imaging will replace echocardiography as an initial imaging test in these patients, it can potentially provide a versatile second-level detailed diagnosis in selected patients. The availability of MR-compatible exercise bikes and wide bore magnet configurations has improved the feasibility of supine MR exercise stress testing. Here, we present an MR imaging study that examines the correlations between LV longitudinal strain and chamber blood velocity during exercise stress in normal volunteers.

It has been shown that precise quantitative measurements of regional and global wall motion can be obtained using MR imaging methods, such as MR tagging (7–11), phase-contrast (12–14) imaging, or stimulated echo imaging (15,16). Phase-contrast methods have also demonstrated the capability to measure chamber blood velocity and quantify transvalvular velocity or regurgitant flows across defective valves (17,18). Typically, these measurements are acquired separately using different pulse sequences and imaging parameters. However, during stress tests in patients, the ability to simultaneously image transient, nonstable physiological manifestations in myocardial motion and transvalvular blood velocity under varying loading conditions may be crucial.

In this study, we employ a recently introduced MR imaging technique called spatial modulation of magnetization acquisitions with encoded gradients for gauging speed (SPAMM n′ EGGS). This method combines tagging and phase-contrast imaging principles to provide simultaneous measurements of LV longitudinal strain and chamber blood velocity for any given LV long-axis slice in a single, short, breath-held acquisition. To our knowledge, no previous study has provided correlated measurements of these two parameters under exercise stress.

[1]Laboratory of Cardiac Energetics, Division of Intramural Research, National Heart, Lung, and Blood Institute, National Institutes of Health, DHHS, Bethesda, Maryland, USA.

[2]ETSI Telecomunicación, Universidad Politécnica de Madrid, Madrid, Spain.

[3]CIBER-BBN, Spain.

Grant sponsor: Intramural Research Program of the National Heart Lung and Blood Institute; Grant number: Z01HL004609; Grant sponsor: Spanish Ministry of Education and the CDTEAM Project from the Ministry of Industry; Grant number: TIN2007-68048-C02-01.

*Correspondence to: Smita Sampath, Ph.D., Department of Diagnostic Radiology, Yale School of Medicine, The Anlyan Center, 300 Cedar Street, N131, New Haven, Connecticut 06520. E-mail: smita.sampath@yale.edu

Received 9 June 2010; revised 16 August 2010; accepted 9 September 2010.

DOI 10.1002/mrm.22668

Published online 4 November 2010 in Wiley Online Library (wileyonlinelibrary.com).

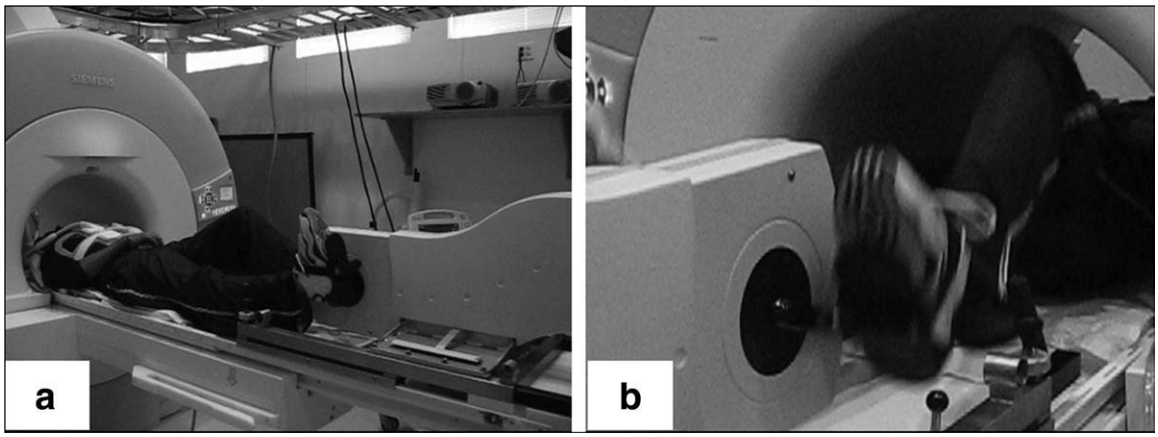

FIG. 1. **a**: Photo depicting the Lode ergometer mounted on the far end of the patient table. The volunteer is lying in the supine head first position. Signal reception is obtained using anterior and posterior two-channel cardiac phased arrays. **b**: Photo depicts clearance of the knee from the upper shroud of the magnet when the patient is moved to the landmark position for scanning.

In this article, as a technical proof of concept of the method, we present such measurements obtained from six normal volunteers during rest, exercise-stress, and post-stress recovery studies.

MATERIALS AND METHODS

Experimental Setup

Experiments were performed in the wide bore 1.5T Espree scanner (Siemens Medical Solutions, Erlangen, Germany) equipped with gradient coils capable of imaging at 33 mT/m and with maximum slew rates of 100 T/m/sec. An MR-compatible bicycle ergometer (Lode Medical Technology, Groningen, Netherlands) was mounted at the furthest position on the foot-end of the patient table (see Fig. 1a). The volunteer was oriented head-first supine on the table and positioned with respect to the bike to ensure clearance of the knees from the upper shroud of the scanner bore during pedaling motion (see Fig. 1b). Anterior and posterior two-channel, phased-array, receive-only torso surface coils (Siemens Medical Solutions, Erlangen, Germany) were employed for all experiments. The volunteer's electrocardiogram (ECG) waveforms were recorded during the rest, stress, and post-stress recovery scans, and noninvasive blood pressure recordings were obtained immediately before and after each scan using an MR-compatible monitoring system (Invivo, Orlando, FL). We recognize that the ECG waveforms obtained are not suitable for diagnosis because of radio frequency (RF) interference. However, the system provided the ability to continuously monitor and record the heart rate and R–R interval during all scans.

Pulse Sequence

For all studies in this article, we employed a recently developed hybrid tagging–phase-contrast pulse sequence called SPAMM n′ EGGS (19) to provide correlated as well as spatially and temporally registered measurements of one-dimensional tissue motion and one-dimensional chamber blood velocity in any desired slice orientation in a single breath-hold.

The pulse sequence timing diagram, with displacement and velocity sensitivities along the readout direction, is shown in Fig. 2. The main features of this sequence include: (1) a 1-1 SPAMM (20) tagging

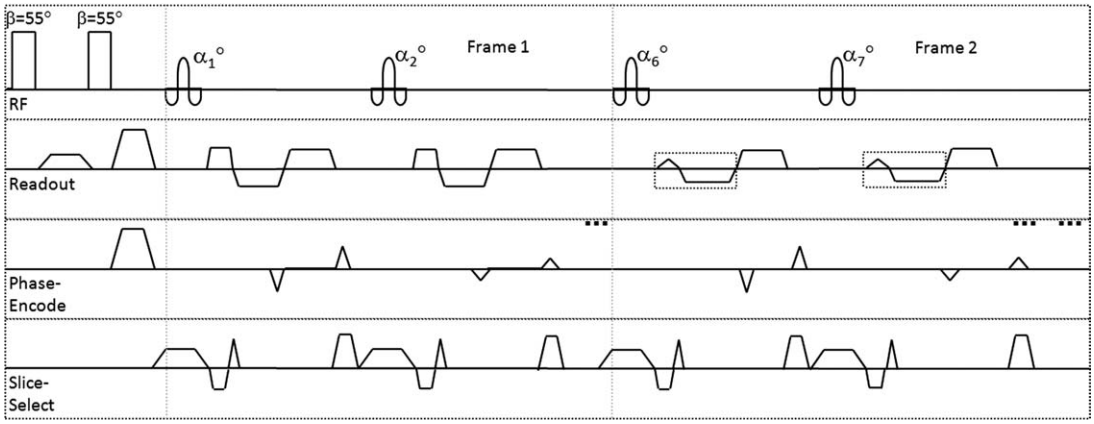

FIG. 2. Pulse sequence timing diagram for the hybrid tagging–phase-contrast imaging pulse sequence (SPAMM n′ EGGS). The rectangular boxes in Frame 2 indicate the bipolar gradient pulses played out before the readout gradient to obtain velocity encoding of chamber blood in addition to the tagged myocardium.

Table 1
Absolute Heart Rate and Heart Rate Relative to Maximum Age Predicted Heart Rate During Rest, Stress, and Post-Stress Recovery For Each Volunteer

	Absolute heart rate (beats/min)			Heart rate relative to maximum age predicted heart rate (220-age) (%)		
Volunteer	Rest	Stress	Post-stress recovery	Rest (%)	Stress (%)	Post-stress recovery (%)
Vol 1	60	110	73	33.33	61.11	40.55
Vol 2	60	95	62	30	47.5	31
Vol 3	70	110	95	35.35	55.55	47.97
Vol 4	75	110	80	40.54	59.45	43.24
Vol 5	66	107	74	35.29	57.21	39.57
Vol 6	65	100	71	34.75	53.47	37.96

preparation triggered by the R-wave to quantify one-dimensional tissue motion, (2) bipolar gradient pulses played out every even cardiac phase before the readout gradient (see rectangular boxes in Fig. 2) to achieve sensitivity to chamber blood velocity, and (3) a gated, sequential, multiphase two-dimensional gradient echo imaging readout. Data were acquired for 90% of the R–R interval. The images corresponding to the odd-numbered cardiac phases are standard 1-1 SPAMM tagged images. The even cardiac phase images bear a velocity-encoded phase term in addition to the motion-related tagging modulation. Blood velocity is reconstructed by performing a sliding window phase-sensitive reconstruction operation with the odd images serving as phase reference images. We currently ignore phase error contributions from concomitant gradients and eddy currents. The typical imaging parameters that were used are: imaging matrix: 192 × 160, receiver bandwidth: ±48 KHz, resolution: 1.6 mm × 1.6 mm, slice thickness: 8–10 mm, echo time: 4.5 msec, repetition time: 7.6 msec, views per cardiac phase: 5, tag separation: 8 mm, and V_{enc}: 90 cm/sec. With these imaging parameters, a temporal resolution of around 38 msec was achieved (the temporal resolution for the blood velocity data is 76 msec, but the data is view-shared to produce an image every 38 msec), resulting in scan durations of 20–25 sec under nonstress conditions and 10–15 sec under stress.

There is a compromise between good tag contrast and imaging signal amplitude for blood velocity encoding. If 90° tagging pulses are used, the mixing of the saturated blood will yield a very low signal in the velocity-encoded image; on the other hand, if low tagging tip angles are used, the tag contrast is poor. We performed a set of numerical simulations to find a good working point for the tagging tip angle and the sequence of imaging flip angles used. A tailored train of imaging flip angles α_i that bear the following relationship with each other was implemented:

$$\alpha_i = a \tan\left(\sin(\alpha_{i+1})e^{-TR/T_1}\right) + (y \times (n-i))/(n-1). \quad [1]$$

The number of imaging RF pulses is denoted by n, and γ is the slope factor for the additive ramp-down function. The family of curves for the tag contrast and blood velocity signal was simulated for a range of (1) tagging tip angle β, (2) imaging final flip angles α_n, and (3) slope factor γ to identify optimal parameter values that maximize the tag contrast persistence and blood pool signal strength during the cardiac cycle. From these simulations, a β of 55°, an α_n of 10−15°, and a γ of 5 were found to provide a good compromise between tag signal fading and blood pool signal relaxation for our typical acquisitions. The strain and velocity curves between a typical SPAMM n′ EGGS acquisition using optimized imaging parameters and standard tagging and phase-contrast acquisitions were compared in our previous study (19) and the results demonstrate close correspondence in measurements.

Data Acquisition

All in-vivo studies were approved by the Institutional Review Board of the National Health, Lung and Blood Institute and informed consent was obtained from all subjects. For each volunteer, long-axis slices in the four-chamber and two-chamber orientations were prescribed. For each slice, a breath-held rest dataset was first acquired. The tags were oriented perpendicular to the long axis, and the blood velocity sensitivity was along the long axis. The exercise bike was programmed to demand a fixed power level so that the volunteer was required to maintain a fixed work rate. The volunteer was first instructed to cycle for about 2 min until a steady-state heart rate (typically twice the resting heart rate) for that workload was attained. The volunteer was then instructed to stop cycling, immediately following which a breath-held stress dataset for one long-axis slice was acquired. The volunteer was finally instructed to resume cycling, and the procedure described earlier was repeated to acquire the second long-axis slice when the same steady-state heart rate was achieved. A decrease in around 5–10% of the steady-state heart rate was observed during the course of the imaging for both long-axis slices. The volunteer was made to rest for 10 min before post-stress recovery datasets for the two slices were acquired. The heart rates at post-stress recovery were higher than the resting heart rates. The absolute heart rate and the heart rate relative to the maximum age predicted heart rate (220-age) during rest, stress (mean heart rate during the image acquisition period), and post-stress recovery for each volunteer is tabulated in Table 1.

Data Analysis

Quantitative measurements of LV regional tissue mechanics, LV regional hemodynamics, and LV geometry were obtained from the acquired SPAMM n′ EGGS datasets.

LV Mechanics

The reconstructed tagged magnitude images were post-processed automatically using a recently published method (21) to obtain average longitudinal strain for the four walls—anterior, posterior (from the two-chamber slice), lateral, and septal (from the four-chamber slice)—in regions of interest (ROIs) selected in the midventricular wall. The postprocessing technique employed uses nonrigid registration between temporally adjacent tagged images to compute the dense myocardial displacement field [see (21) for more details]. Figure 4a-row 1 shows these ROIs for an end-diastolic time frame, while Fig. 4a-row 2 shows these tracked ROIs for an end-systolic time frame. For each volunteer, the average longitudinal strain from the four walls was computed and plotted (see markers in Fig. 4b). A spline interpolated smooth strain curve was also computed and overlaid (see solid line in Fig. 4b). Strain-rate curves were then obtained by computing sliding two-point time derivatives of normalized smooth strain curves (see dashed line in Fig. 4b). The average slope of the strain-rate curve was computed, and the time to peak longitudinal strain was measured as the time of zero-crossing of the strain-rate curve.

LV Hemodynamics

For each volunteer, ROIs were manually defined to best capture LV outflow velocity (see rectangular boxes marked 1 and 2 in Fig. 5a) and the mitral inflow velocity (see rectangular boxes 3 and 4 in Fig. 5b) on the reconstructed blood velocity images. For all time points during systole, aortic outflow velocity was computed by averaging the blood velocity in all the pixels that lie within boxes 1 and 2. For all time points during diastole, mitral inflow velocity was computed by averaging the blood velocity in all the pixels that lie within boxes 3 and 4. A composite smooth velocity–time curve was then generated by spline interpolating these points. Acceleration curves were then obtained by computing sliding two-point time derivatives of the velocity curves. Time to peak mitral inflow velocity was measured as the time of second zero-crossing of the acceleration curve (see Fig. 5c).

Strain–Velocity Inter-Relationships

The time interval between peak longitudinal strain (zero-crossing of the strain-rate curve) and peak mitral inflow velocity (zero-crossing of the acceleration curve) was then computed (T_{ps-pf}), and the percentage of longitudinal relaxation (S_{ps-pf}) that occurs during this time interval was computed for each volunteer.

LV Geometry

An estimate of ventricular volume was computed for each volunteer from the two long-axis slices using the biplane area length method (22). The inner walls were manually contoured, and the areas of the LV chamber were computed for the two-chamber (A_1) and the four-chamber (A_2) slice orientations. The long-axis distance from the mitral valve plane to the apex was also measured (l_1 and l_2). From these measurements, the ventricular volume (V) was then computed using the formula: $V = [0.85 \times A_1 \times A_2]/[0.5 \times (l_1 + l_2)]$ for all time frames. From measurements of end-diastolic volume and end-systolic volume, global measures such as ejection fraction and cardiac output were also computed for all six volunteers.

Statistics

For the data pool obtained from the six volunteers, two-tailed paired t-test statistical analysis was performed to determine difference in means of measured parameters between rest and stress at the significance level of $P < 0.05$. For the time-related terms, to account for intersubject variability in R–R intervals, results were computed as % of R–R interval for all volunteers. The parameters analyzed were: (1) peak systolic longitudinal strain, (2) slope of the strain-rate curve, (3) time to peak strain, (4) peak mitral inflow velocity, (5) time to peak mitral inflow velocity, (6) time from peak strain to peak mitral inflow velocity (T_{ps-pf}), (7) percentage longitudinal relaxation at peak mitral inflow velocity (S_{ps-pf}), (8) ejection fraction, and (9) cardiac output.

RESULTS

The combined tag-blood velocity maps obtained during rest, stress, and post-stress recovery in a two-chamber long-axis slice from a representative volunteer are depicted in Fig. 3 for every alternate time frame beginning with the second one. In total, sixteen time frames during rest and post-stress recovery and ten time frames during stress were acquired covering 90% of the R–R interval. From the figures, it is evident that during stress, there is an early initiation of rapid aortic outflow velocity (see arrows in yellow), early occurrence of peak end-systolic longitudinal strain (see rectangular boxes), and higher peak mitral inflow velocities (see arrows in orange). We also note that the post-stress recovery images resemble the rest images quite closely.

Figures 4–6 provide a more detailed quantitative description of the temporal behavior of the midventricular longitudinal strain and strain rate, transvalvular velocity, and ventricular volume. Figure 4b shows the average longitudinal strain evolution curves computed from four midventricular ROIs as defined on the four walls in Fig. 4a. Row 1 in Fig. 4a depicts the ROIs during end-diastole, while row 2 in Fig. 4a depicts the position of these tracked ROIs during end-systole. The shape of the curve in Fig. 4b is typical with longitudinal shortening during systole, followed by longitudinal relaxation during diastole. The computed strain rate curves are overlaid for reference, and a vertical line was plotted to mark the time intercept of the strain-rate curve or the time to peak longitudinal strain (around 266 msec). Figure 5c depicts the quantitative composite blood velocity curves. The portion of these curves before zero-crossing is the average aortic outflow velocity from ROIs marked 1 and 2 in Fig. 5a, while the portion of the curves post zero-crossing is the average mitral inflow velocity from ROIs marked 3 and 4 in Fig. 5b. The computed acceleration

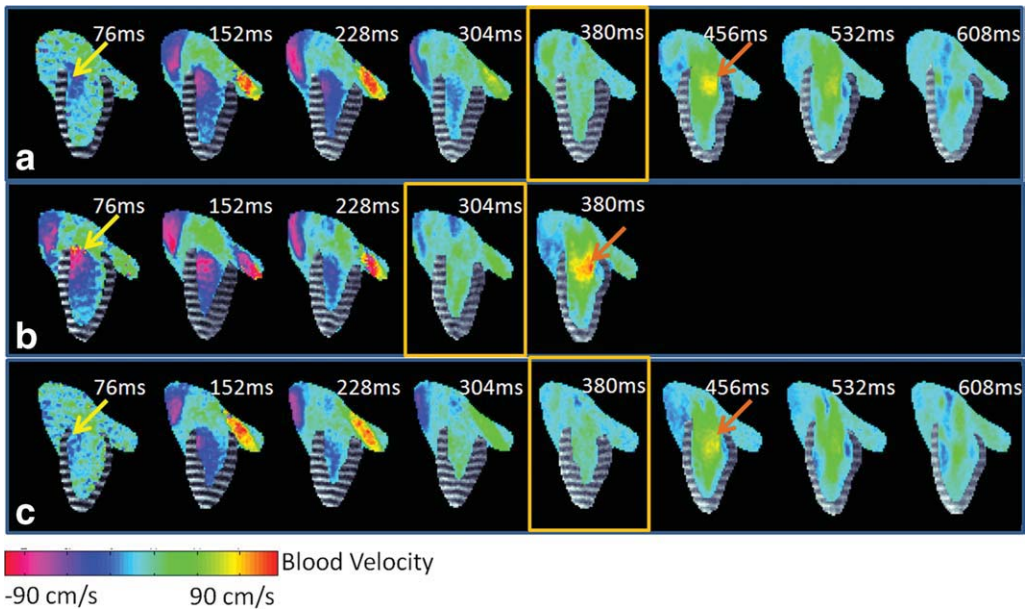

FIG. 3. Combined tagged myocardium and blood velocity maps during (**a**) rest, (**b**) stress, and (**c**) post-stress recovery in one normal volunteer using SPAMM n′ EGGS. The velocity is color-coded in accordance with the color-bar. The blood velocity maps reveal early initiation of aortic flow during stress (yellow arrows) and increased mitral inflow velocities during stress (orange arrows). The tagged myocardium reveals earlier occurrence of end-systolic peak longitudinal shortening during stress (yellow boxes).

curves are overlaid for reference, and a vertical line was plotted to mark the second time intercept of the acceleration curve or the time to peak mitral inflow velocity (around 442 msec).

Figure 6 displays combined strain, blood velocity, and volume curves for (a) rest, (b) stress, and (c) post-stress recovery. Vertical lines, obtained from zero-crossings of strain-rate and acceleration curves, respectively, are overlaid on each plot to mark peak longitudinal strain and peak mitral inflow velocity. Comparing the three curves, the time interval from peak longitudinal strain to peak mitral inflow velocity ($T_{\mathrm{ps-pf}}$) was found to be maintained during stress, while the percentage of longitudinal relaxation during this period ($S_{\mathrm{ps-pf}}$) increased with stress because of increased rates of longitudinal relaxation. In this volunteer, the peak longitudinal strain was also higher during stress, but this was not found to be statistically true across all volunteers. The mitral inflow velocity was statistically higher during stress than rest. The volume curves indicate a decrease in ventricular volume during systole and an increase in ventricular volume during diastolic rapid filling as expected. The volume curves achieve their minimum value shortly after peak longitudinal strain and begin to increase around the zero-

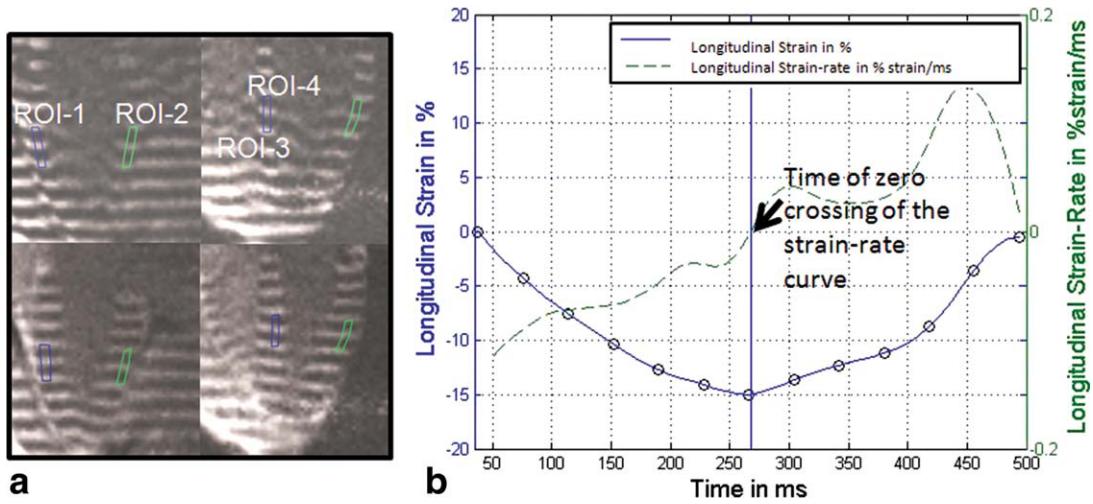

FIG. 4. **a**: Figures showing the position of the four midventricular regions of interest at end-diastole (row 1) and at end-systole (row 2) on the two-chamber (column 1) and the four-chamber (column 2) slice orientations. **b**: Average midventricular longitudinal strain and corresponding strain-rate curves. Note the time of peak longitudinal strain indicated by the superimposed vertical line at the zero-crossing of the strain-rate curve. Curves are generated using datasets from a representative volunteer obtained during rest.

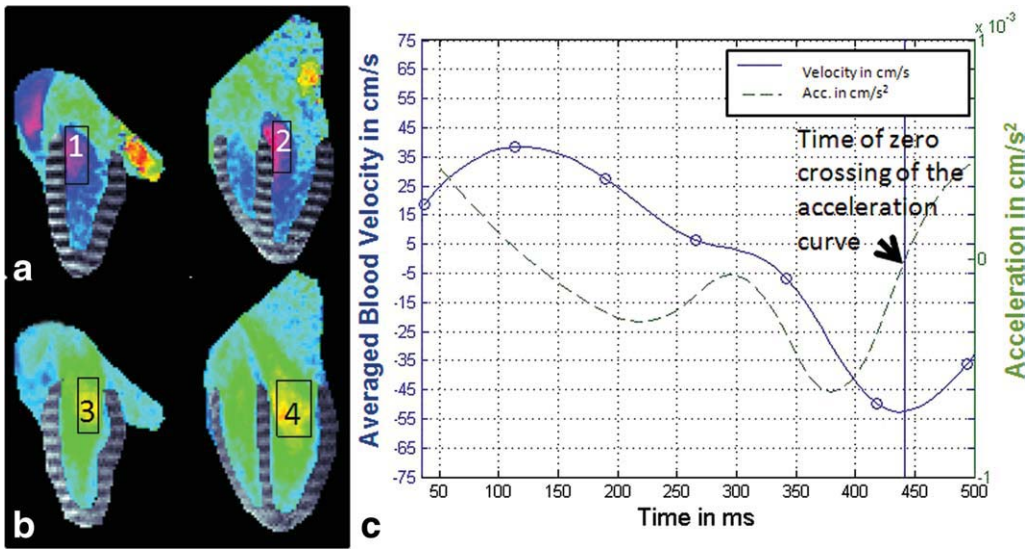

FIG. 5. **a**: Figures showing the position of the aortic outflow region of interest on a two-chamber and a four-chamber slice. **b**: Figures showing the position of the mitral inflow region of interest on a two-chamber and a four-chamber slice. **c**: Composite blood velocity curves depicting the evolution of aortic outflow velocity (average velocity in ROIs depicted in a) and mitral in-flow velocity (average velocity in ROIs depicted in b) in a normal volunteer and corresponding acceleration curves. Note the time of peak mitral inflow velocity indicated by the superimposed vertical line at the second zero-crossing of the acceleration curve. Curves are generated using datasets from a representative volunteer obtained during rest.

crossing of the blood velocity curve. The isovolumic relaxation time (time interval between the vertical dashed lines in Fig. 6) is found to be shorter during stress as compared with rest, indicating increased rate of pressure decay within the LV during exercise. The start of isovolumic relaxation is also shifted in time relative to peak longitudinal strain during stress. The volume curves on their own provide limited information in comparing rest versus stress curves, highlighting the importance of functional data over geometric data in this scenario.

The quantitative results for nine parameters that characterize the behavior of these curves for all six volunteers are presented in Table 2. The values are displayed as mean ± standard deviation. Of these parameters, we find that the slope of the strain-rate curve, the time to peak longitudinal strain, peak mitral inflow velocity, the time to peak mitral inflow velocity, and cardiac output are significantly different during stress as compared with the rest studies at the 0.05 level for a two-tailed paired student's t-test. These results validate previous studies in the Echocardiography literature. In addition, as a result of simultaneous strain and blood velocity measurements, two additional parameters T_{ps-pf} and S_{ps-pf} were investigated. Although T_{ps-pf} was shorter during stress as compared with rest, this was not found to be statistically significant at the 0.05 level. However, S_{ps-pf} was found to be significantly higher during stress as compared with rest at the 0.05 level. The statistical tests were carried out after the parameters were normalized across subjects for differential resting heart rates.

DISCUSSION

We have successfully demonstrated the feasibility of performing a comprehensive examination of cardiac mechanics and hemodynamics during supine bicycle exercise tests in a wide bore MR scanner using a hybrid tagging–phase-contrast imaging pulse sequence, SPAMM n′ EGGS. The MR-compatible bicycle ergometer permits data acquisition in the MR scanner soon after peak exercise stress with minimum delay. The results are very encouraging and depict significant alterations in amplitude and temporal behavior of certain physiological parameters during exercise-stress in normal volunteers. We believe that such studies may prove to be beneficial in the clinical diagnostic examination of patients with cardiac disease.

By combining the measurements using our hybrid method, a two-fold reduction in acquisition time is obtained. Further, the blood velocity and myocardial strain data obtained for any given slice is spatially and temporally registered, thus accounting for changes in patient position from one postexercise breath-hold to another. Here, we acquire two long-axis slices in two separate breath-holds. In the future, we hope to use parallel imaging schemes to enable both these acquisitions in a single breath-hold. Since the blood velocity and myocardial strain data are acquired simultaneously, any transient physiological events, such as induced stress, are manifested in a correlated fashion on both datasets.

Doppler tissue imaging has been used to study regional patterns of myocardial strain and strain rates during rest and exercise stress (23,24). These studies have reported limitations of reproducibility in regional strain measurements because of the inherent angle dependency of the ultrasound beam. Studies have also reported difficult apical windows, poor data quality in the lateral and anterior wall potentially due to shadowing by the lung. MR tagging allows the regional quantification of myocardial strain in any slice orientation and any region with

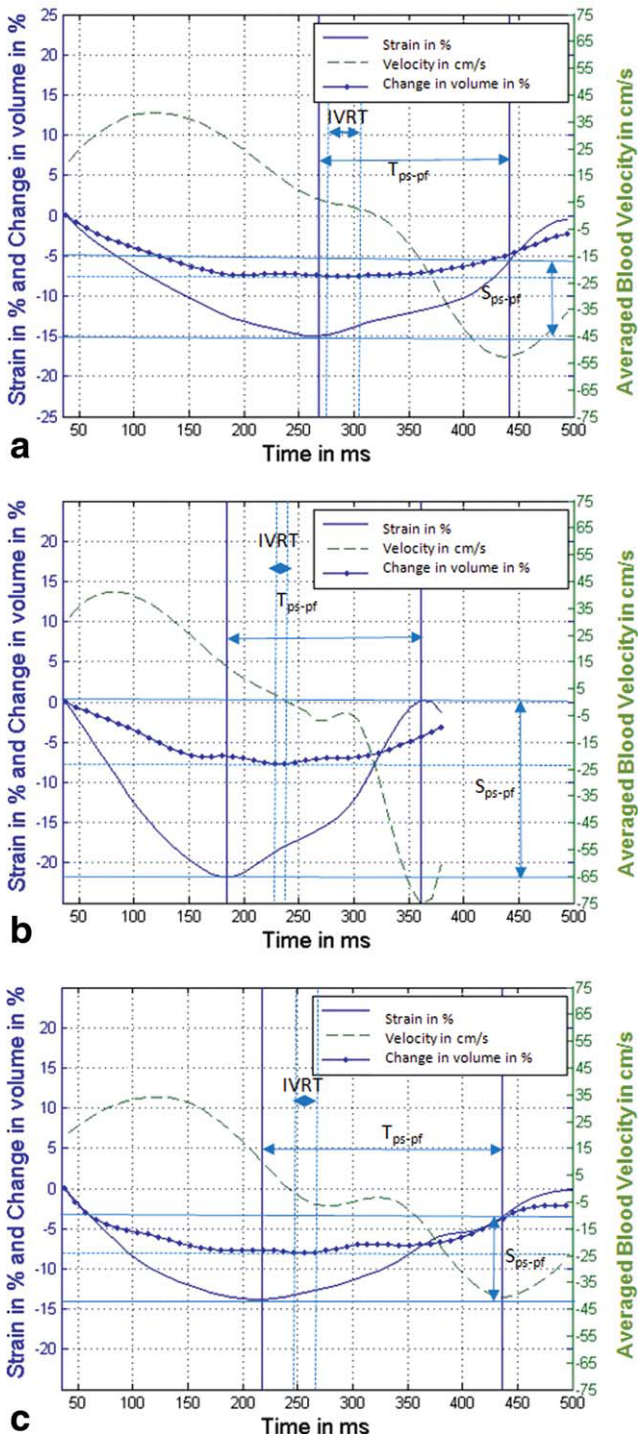

FIG. 6. Longitudinal strain, composite transvalvular flow velocity, and volume curves for (**a**) rest, (**b**) stress, and (**c**) post-stress recovery. Note vertical lines superimposed at time of peak strain and time of peak mitral inflow velocity. The time interval between peak strain to peak mitral inflow velocity (T_{ps-pf}) is maintained, while the percentage relaxation of strain (S_{ps-pf}) during T_{ps-pf} is increased during stress. Curves are generated using datasets from a representative volunteer.

excellent reproducibility. In this study, we have reported longitudinal strain and strain rates in the midventricle. Our results demonstrate no increase in peak strain but an increase in strain-rate values during stress—comparable to the results presented in previous Doppler tissue imaging studies (23). More recently, diastolic function during exercise has been studied using a combination of color Doppler flow to quantify mitral inflow velocity and Doppler tissue imaging to quantify mitral annular longitudinal velocities (25). The mitral annular velocity is chosen over regional myocardial strain evaluation because the location of the mitral annulus can be easily identified. As a result, the ultrasound beam can be aligned perpendicular to the annulus during the scan resulting in high reproducibility of the mitral annular longitudinal velocities. These studies have focused on investigating changes in the ratios of the peak mitral inflow velocity to the peak mitral annular velocity. This represents a more global estimate of diastolic function. Using the SPAMM n′ EGGS method, we can obtain a region-by-region estimate of diastolic function with high reproducibility. In this article, we focus on quantifying strain in the midventricular region, but the method can be used to investigate strain–velocity relationships in any ROI. In addition, since the datasets are acquired simultaneously, the SPAMM n′ EGGS method enables the study of the relative timings between the regional strain curves and mitral inflow velocity curves, which provides new information regarding changes in diastolic filling periods. We also measure the percentage of longitudinal relaxation that occurs at peak mitral inflow velocity. This parameter sheds insight on regional myocardial material properties during passive diastolic filling.

Rest Versus Stress

LV response to the stress of exercise typically involves a complicated interaction between heart rate, contractility, and loading conditions. From our results, we observe a significant increase in (1) cardiac output, (2) slope of the strain-rate curve, and (3) peak mitral inflow velocity during exercise stress. In addition, the time interval from peak longitudinal strain to peak mitral inflow velocity (T_{ps-pf}) remained statistically constant under stress; however, the percentage of longitudinal relaxation during this period (S_{ps-pf}) increased with stress. The consequence of this was that peak mitral inflow velocity during stress occurred when the LV had fully relaxed, whereas during rest, the peak velocity occurred during the final phase of LV relaxation. No significant changes in stroke volume or ejection fraction were observed. These results demonstrate a link between exercise stress and diastolic performance. During exercise, there is a marked increase in heart rate, resulting in a shorter diastole. However, the stroke volume and ejection fraction are maintained through an augmentation in contractility and filling efficiency. This is achieved through increased relaxation strain rates leading to increased suction, increased peak mitral inflow velocities, and maintenance of early diastolic filling timings. A combination of these effects during early diastole contributes toward early relaxation and near restoration of end-diastolic volume despite a shorter diastole. Albeit, an increase in stroke volume was not observed in this study. This was because the augmentation in filling efficiency and increased

Table 2
Mean and Standard Deviation of Left Ventricular Mechanical and Hemodynamic Parameters Computed During Rest, Stress, and Post-Stress Recovery in a Pool of Six Volunteers

	Rest (mean ± standard deviation)	Peak stress (mean ± standard deviation)	Post-stress recovery (mean ± standard deviation)
Peak systolic strain (%)	−15.36 ± 1.71	−15.23 ± 1.83	−15.39 ± 1.46
Slope of strain rate curve	0.025 ± 0.002	0.049 ± 0.010[a]	0.031 ± 0.006
Time to peak strain (% R–R interval)	33.28 ± 1.86	25.70 ± 2.12[a]	30.92 ± 2.36
Peak inflow velocity (cm/sec)	−71.45 ± 21.90	−107.20 ± 36.25[a]	−60.62 ± 15.54
Time to peak mitral inflow velocity (% R–R interval)	44.37 ± 5.21	35.50 ± 4.19[a]	44.37 ± 5.21
Time interval from peak strain to peak mitral inflow velocity, T_{ps-pf} (% R–R interval)	16.55 ± 3.23	13.40 ± 3.06	20.12 ± 4.72[b]
Percent longitudinal relaxation from peak strain to peak mitral inflow velocity, S_{ps-pf}	63.46 ± 7.72	84.32 ± 6.24[a]	64.16 ± 8.99
Ejection fraction (%)	71.70 ± 9.10	72.86 ± 6.03	79.30 ± 4.36[b]
Cardiac output (L/min)	5.31 ± 0.94	6.71 ± 1.22[a]	5.72 ± 1.05

[a]Rest versus stress statistically different at $P < 0.05$ level for a two-tailed t-test.
[b]Rest versus post-stress recovery statistically different at $P < 0.05$ level for a two-tailed t-test.

preload was not sufficient to increase end-diastolic volume compared with resting values at the operating workload and increased heart rates. Parameters that shed insight into abnormalities in such inter-relationships between diastolic relaxation and filling patterns during exercise stress may provide a more sensitive and comprehensive diagnosis in patients presenting with diastolic dysfunction.

Post-Stress Recovery

Our post-stress recovery measurements illustrate compensatory adjustments to normalize cardiac function to resting values. For all six volunteers, we observed that the heart rate during recovery was lower than during stress but were still higher than resting conditions. We observed an increase in stroke volume and ejection fraction during recovery compared with resting values. This was due to decreased end-systolic volumes during recovery compared with resting conditions. We also observed an increase in stroke volume and ejection fraction compared with stress values. This was due to the decrease in the heart rate during recovery as compared with stress resulting in higher end-diastolic volumes during recovery. The cardiac output, however, was lower during recovery compared with stress conditions indicating that the increase in stroke volume during recovery did not compensate for the increase in heart rate during stress. We also observed that the rate of change in strain and strain rate during recovery is lower than stress but were higher than during resting conditions. This decrease in strain rate is likely because of the reduction in the sympathetic tone during recovery. From the strain-rate patterns, we would expect that end-systolic LV suction is lower during recovery compared with stress but higher compared with resting states. However, the mitral inflow velocities during recovery were lower than those at rest. This could potentially be the result of a decreased preload because of the shorter isovolumic relaxation times during recovery compared with resting conditions. The time from peak strain to peak mitral inflow velocity T_{ps-pf} was longer during recovery, indicating longer filling times required to achieve increased stroke volume. Patterns of heart rate recovery post-stress have been shown to provide an independent prediction of outcome (26). Studying the relationships between strain, volume, and blood velocity during cardiac recovery post-stress may provide crucial prognosis in select patients.

Limitations

In this study, we focus on the diastolic inter-relationships between midventricular average longitudinal strain and mitral inflow velocity as a first step. In the future, these methods could be extended to study the systolic and diastolic inter-relationships between strain patterns across multiple regions (basal, apical and mid; and anterior, posterior, lateral, and septal) and multidirectional sensitivity (longitudinal, circumferential, and radial) and their interactions with both velocity peaks (aortic outflow and mitral inflow).

We recognize that while our velocity sensitive direction is along the direction of the maximum mitral inflow velocity vectors, it is not along the direction of the maximum outflow velocity vectors. As a result, our aortic outflow velocity measurements are a projection of the peak outflow velocity vectors along the long axis of the imaged slice. In the future, with faster acquisition or free-breathing strategies, we may be able to acquire both in-plane velocity measurements, which will enable us to compute the outflow velocity vectors oriented along the direction of the outflow tract.

Our study is also limited by the temporal resolution of the method—which may result in underestimation of strain, especially during stress. In the future, scaling the temporal resolutions during stress acquisitions proportionately with the increase in heart rates would be ideal.

We ignore phase error contributions from concomitant gradients in this study. In the future, applying opposite polarity bipolar gradients every alternate frame will enable reduction of these artifacts by canceling effects from square gradient terms.

The SPAMM n′ EGGS imaging sequence has diagnostic potential in exercise stress testing of patients with

cardiac disease. The data acquired may be able to detect regions of altered myocardial contractility and quantify flow abnormalities in response to exercise stress. Regional dyssynchrony between myocardial segments, or dyssynchrony in the relative timings of the mechanical and hemodynamic curves, e.g., changes in filling periods, can be measured and may provide additional diagnostic information in select patient groups.

CONCLUSIONS

We have been able to conclusively demonstrate that sensitive measures of regional cardiac mechanics and hemodynamics during exercise stress can be obtained in an MR scanner using a combined tagging–phase-contrast imaging pulse sequence.

ACKNOWLEDGMENTS

The authors thank Dr. Andrew Arai for his support and medical coverage during the scans. This work was supported by the Intramural Research Program of the National Heart Lung and Blood Institute (PI: E.R. McVeigh). Dr. Ledesma-Carbayo's efforts were partially supported by the research project from the Spanish Ministry of Education and the CDTEAM project from the Ministry of Industry.

REFERENCES

1. Lancellotti P, Lebrun F, Pierard LA. Determinants of exercise-induced changes in mitral regurgitation in patients with coronary artery disease and left ventricular dysfunction. J Am Coll Cardiol 2003; 42:1921–1928.
2. Lancellotti P, Troisfontaines P, Toussaint AC, Pierard LA. Prognostic importance of exercise-induced changes in mitral regurgitation in patients with chronic ischemic left ventricular dysfunction. Circulation 2003;108:1713–1717.
3. Pierard LA, Lancellotti P. Stress testing in valve disease. Heart 2007; 93:766–772.
4. Wu WC, Aziz GF, Sadaniantz A. The use of stress echocardiography in the assessment of mitral valvular disease. Echocardiography 2004; 21:451–458.
5. Davidavicius G, Kowalski M, Williams RI, D'Hooge J, Di Salvo G, Pierre-Justin G, Claus P, Rademakers F, Herregods MC, Fraser AG, Pierard LA, Bijnens B, Sutherland GR. Can regional strain and strain rate measurement be performed during both dobutamine and exercise echocardiography, and do regional deformation responses differ with different forms of stress testing? J Am Soc Echocardiogr 2003;16:299–308.
6. Dagianti A, Penco M, Agati L, Sciomer S, Rosanio S, Fedele F. Stress echocardiography: comparison of exercise, dipyridamole and dobutamine in detecting and predicting the extent of coronary artery disease. J Am Coll Cardiol 1995;26:18–25.
7. Axel L, Goncalves RC, Bloomgarden D. Regional heart wall motion: two-dimensional analysis and functional imaging with MR imaging. Radiology 1992;183:745–750.
8. McVeigh ER. MRI of myocardial function: motion tracking techniques. Magn Reson Imaging 1996;14:137–150.
9. Zerhouni EA, Parish DM, Rogers WJ, Yang A, Shapiro EP. Human heart: tagging with MR imaging—a method for noninvasive assessment of myocardial motion. Radiology 1988;169:59–63.
10. Osman NF, McVeigh ER, Prince JL. Imaging heart motion using harmonic phase MRI. IEEE Trans Med Imaging 2000;19:186–202.
11. Osman NF, Prince JL. Visualizing myocardial function using HARP MRI. Phys Med Biol 2000;45:1665–1682.
12. Meyer FG, Constable RT, Sinusas AJ, Duncan JS. Tracking myocardial deformation using phase contrast MR velocity fields: a stochastic approach. IEEE Trans Med Imaging 1996;15:453–465.
13. Pelc LR, Sayre J, Yun K, Castro LJ, Herfkens RJ, Miller DC, Pelc NJ. Evaluation of myocardial motion tracking with cine-phase contrast magnetic resonance imaging. Invest Radiol 1994;29:1038–1042.
14. Reese TG, Feinberg DA, Dou J, Wedeen VJ. Phase contrast MRI of myocardial 3D strain by encoding contiguous slices in a single shot. Magn Reson Med 2002;47:665–676.
15. Aletras AH, Balaban RS, Wen H. High-resolution strain analysis of the human heart with fast-DENSE. J Magn Reson 1999;140:41–57.
16. Aletras AH, Ding S, Balaban RS, Wen H. DENSE: displacement encoding with stimulated echoes in cardiac functional MRI. J Magn Reson 1999;137:247–252.
17. Kilner PJ, Gatehouse PD, Firmin DN. Flow measurement by magnetic resonance: a unique asset worth optimising. J Cardiovasc Magn Reson 2007;9:723–728.
18. Kozerke S, Schwitter J, Pedersen EM, Boesiger P. Aortic and mitral regurgitation: quantification using moving slice velocity mapping. J Magn Reson Imaging 2001;14:106–112.
19. Sampath S, Kim JH, Lederman RJ, McVeigh ER. Simultaneous imaging of myocardial motion and chamber blood flow with SPAMM n′ EGGS (spatial modulation of magnetization with encoded gradients for gauging speed). J Magn Reson Imaging 2008;27:809–817.
20. Young AA, Axel L. Three-dimensional motion and deformation of the heart wall: estimation with spatial modulation of magnetization—a model-based approach. Radiology 1992;185:241–247.
21. Ledesma-Carbayo MJ, Derbyshire JA, Sampath S, Santos A, Desco M, McVeigh ER. Unsupervised estimation of myocardial displacement from tagged MR sequences using nonrigid registration. Magn Reson Med 2008;59:181–189.
22. Underwood SR, Gill CR, Firmin DN, Klipstein RH, Mohiaddin RH, Rees RS, Longmore DB. Left ventricular volume measured rapidly by oblique magnetic resonance imaging. Br Heart J 1988;60:188–195.
23. Pierre-Justin G, Lancellotti P, Pierard LA. What indices quantify regional myocardial function during supine bicycle in healthy subject: natural strain and strain rate? Int J Cardiol 2005;102:21–31.
24. Reuss CS, Moreno CA, Appleton CP, Lester SJ. Doppler tissue imaging during supine and upright exercise in healthy adults. J Am Soc Echocardiogr 2005;18:1343–1348.
25. Peteiro J, Pazos P, Bouzas A, Pinon P, Estevez R, Castro-Beiras A. Assessment of diastolic function during exercise echocardiography: annulus mitral velocity or transmitral flow pattern? J Am Soc Echocardiogr 2008;21:178–184.
26. Gibbons RJ. Abnormal heart rate recovery after exercise. Lancet 2002; 359:1536–1537.